

Dynamic structure of electrons in Li metal: Inelastic synchrotron x-ray scattering results and interpretation beyond the random-phase approximation

W. Schülke, H. Nagasawa, S. Mourikis, and P. Lanzki

Institute of Physics, University of Dortmund, D-4600 Dortmund 50, Federal Republic of Germany

(Received 2 August 1985; revised manuscript received 23 January 1986)

The dynamic structure factor $S(\mathbf{q}, \omega)$ of electrons in Li-metal single crystals for $\mathbf{q} \parallel [100]$, $\mathbf{q} \parallel [110]$, and $\mathbf{q} \parallel [111]$ with $0.28 \text{ a.u.} < q < 1.4 \text{ a.u.}$ was measured with 1-eV resolution by using inelastic scattering of synchrotron x radiation from DORIS II (Doppel-Ring Speicheranlage). Mainly for $q > q_c$ (q_c is the plasmon cutoff vector) the fine structure of $S(\mathbf{q}, \omega)$ exhibits a strong dependence on the direction of the momentum transfer \mathbf{q} . This crystal-lattice-induced peak structure is connected with minima of the combined density of states as due to band gaps across Bragg planes and can be interpreted as zone-boundary collective states within the limits of a two-band approximation. Comparison of the experimental results with model calculations of $S(\mathbf{q}, \omega)$, going beyond the random-phase approximation (RPA) by means of local-field corrections and also taking into account momentum-dependent lifetime effects for the inhomogeneous case (including band-structure effects) led to the following conclusions: (1) Most of the fine structure of $S(\mathbf{q}, \omega)$ is induced by the interaction of electrons with the ion lattice. (2) The overall shape of the $S(\mathbf{q}, \omega)$ spectra, mainly their strong deviation from corresponding homogeneous RPA results, is dominated by the momentum dependence of the inverse lifetime of quasiparticles with a steep rise at momentum p_0 which makes possible decay of quasiparticle states into a plasmon. (3) The influence of exchange and correlation on $S(\mathbf{q}, \omega)$ via a local-field correction factor is found to be appreciable.

I. INTRODUCTION

Despite many experimental and theoretical efforts addressing the behavior of the dynamic structure factor $S(\mathbf{q}, \omega)$ of an inhomogeneous strongly correlated electron liquid at metallic densities, the results of these investigations still disagree. Therefore, this important and interesting problem in many-body physics has to be considered unsolved so far.

One of the most important difficulties on the experimental side of the problem is the appropriate interpretation of inelastic electron scattering data, even when using high-energy electrons. For a momentum transfer q larger than q_c , the plasmon cutoff vector, that part of the scattered spectrum which is due to the dynamic structure factor of bulk electrons, is superimposed by many other features of multiscattering events mixing (quasi)elastic, surface-plasmon, and volume-plasmon scattering, so that it is even very difficult to identify peaks of the dynamic structure factor, especially when a multipoint structure cannot be excluded. Moreover, it seems to be entirely impossible to separate all contributions of the inelastic electron spectra in a unique way in order to obtain the complete information about $S(\mathbf{q}, \omega)$. The interpretation of inelastic electron scattering experiments on Al can be considered as an example of a fundamental disagreement among different authors. Thus, Zacharias¹ has found a peak in the loss spectra of Al, the energetic position of which became constant as a function of q for $q > q_c$, contrary to the predictions of the random-phase approximation (RPA), so that a possible breakdown of the RPA has been suggested. On the other hand, by using more sophisticated data processing, Batson, Chen, and Silcox² have

observed a peak, which follows the predictions of the RPA, whereas Zacharias's peak has been attributed to multiple scattering. Finally the findings of Höbberger, Otto, and Petri³ on Al for $q > q_c$ are between those of Zacharias¹ and Batson *et al.*² as far as the position of that peak is concerned, which is continuing the plasmon peak into the electron-hole continuum. Therefore, one has to admit that even the validity or the breakdown of the RPA in representing the dynamical structure factor of simple metals for $q > q_c$ could not be verified unambiguously.

Possible crystal-lattice effects (electron-ion interaction), which have to be taken into account when one is testing the validity of any approach to the dynamic structure of electrons in crystalline solids, will further make difficult the interpretation of electron-energy-loss results. In the case of Al, the best investigated simple metal, Petri and Otto⁴ and also Chen and Silcox⁵ have reported about special energy-loss peaks on single-crystal Al for scattering vectors parallel to the [100] direction, which have been interpreted by Sturm and Oliveira⁶ as so-called zone-boundary collective states (ZBCS), first introduced by Foo and Hopfield⁷ as due to an excitation gap for excitations across the energy gap at a zone boundary.

A second source of experimental evidence for the dynamical structure factor is inelastic x-ray scattering. Thus further difficulties on the experimental side of the problem with $S(\mathbf{q}, \omega)$ of simple metals arise from the limitations of conventional x-ray source experiments, which are connected both with low photon flux in the scattered beam and low-energy resolution of the x-ray measurements compared with electron-energy-loss experiments. Even when using high-power rotating-anode generators, both the energy resolution of inelastic x-ray scattering ex-

periments performed so far and the signal-to-background ratio are limited by the requirement of using unmonochromatized characteristic x-ray lines with rather large natural width and contaminated by bremsstrahlung. On the other hand, the x-ray measurements are much less influenced by multiscattering events, so that the spectra can give direct evidence of the full shape of $S(\mathbf{q}, \omega)$.

The most prominent feature of dynamic structure factors of simple metals for $q > q_c$, as measured by means of conventional x-ray scattering by Platzman and Eisenberger⁸ on Be, Al, and graphite, by Eisenberger, Platzman, and Schmidt,⁹ by Schülke and Lautner,¹⁰ and by Priftis, Boviatsis, and Vradis¹¹ on Li, is a fine structure with at least two peaks (double-peak structure), where one peak exhibits nearly no dispersion and the other one follows roughly the free-electron RPA peak. This "universal double peak structure," which has been interpreted by Platzman and Eisenberger⁸ as an indication of an incipient Wigner electron lattice, has prompted much theoretical work. These theoretical activities looked for universal properties of the strongly correlated electron liquid in spite of the fact that the energy resolution of the x-ray experiments, together with their statistical accuracy, do not seem to be sufficient to rule out that lattice effects (ZBCS's) can be superimposed on more or less "universal structures."

Most recent inelastic x-ray scattering experiments on single-crystal Li using synchrotron radiation done by Schülke, Nagasawa, and Mourikis¹² have given strong evidence that the fine structure of $S(\mathbf{q}, \omega)$ for $q > q_c$ is heavily influenced by electron-ion interaction. As will be stressed at the end of this section, this kind of experiment should give the best insight into all effects influencing $S(\mathbf{q}, \omega)$, since it connects both sufficient energy resolution and statistical accuracy, as far obtained only with electrons, with almost complete absence of multiscattering events.

It has been already mentioned that not only the experimental situation, with respect to $S(\mathbf{q}, \omega)$, of simple metals seems to be rather confusing. Also the theoretical effort, prompted by the experimental findings, has not come to a consistent result.

As far as the "universal double-peak structure" is concerned, first Mukhopadhyay, Kalia, and Singwi¹³ were able to reproduce such a double peak structure of $S(\mathbf{q}, \omega)$ by introducing damping of the single-particle states via the self-energy into the theory of Vashishta and Singwi,¹⁴ which goes beyond RPA by taking into account explicitly the short-range and correlation hole around each electron (local-field correction). The objections of Rao, Mandl, and Tripathy¹⁵ against this scheme seem to be erroneous, as has been pointed out by Rahman and Vignale¹⁶ most recently. The latter authors, as well as Niklasson, Sjölander, and Yoshida¹⁷ have stressed that it is the momentum dependence of the lifetime of excited quasi-particles which generates the double-peak structure of $S(\mathbf{q}, \omega)$. A steep rise of the inverse lifetime is predicted at a momentum which makes possible decaying by emitting of a plasmon. Also Awa, Yasuhara, and Asaki¹⁸ have successfully reproduced the double-peak structure when introducing lifetime effects into their diagrammatic ap-

proach via self-energy. The application of Mori's¹⁹ memory-function formalism to the calculation of $S(\mathbf{q}, \omega)$ (Refs. 20 and 21) did not reveal the double-peak structure unless free-parameter adjustment without clear physical significance has been utilized.²¹

Other many-body schemes have been tried to reproduce the fine structure in $S(\mathbf{q}, \omega)$, as the boson formulation of interacting fermion systems of Pajanne,²² or the formalism of Green, Lowy, and Szymanski²³ and of Green, Neilson, and Szymanski,²⁴ which takes care of short-range correlation of electron pairs. Although these authors found some fine structure in $S(\mathbf{q}, \omega)$, there was no convincing agreement with experiment as far as the position of fine structural details is concerned. Nevertheless, the latter authors obtained a rather good agreement with experiment¹¹ for Li with respect to the overall shape of the spectra.

Equation-of-motion schemes for density operators as applied by Utsumi and Ichimaru to $S(\mathbf{q}, \omega)$ failed to reproduce the double-peak structure.²⁵ The apparent general validity of a double-peak structure in $S(\mathbf{q}, \omega)$ of simple metals has kept away most of the authors to look for crystal lattice effects as one possible reason for this fine structure. Additionally, the applicability of weak pseudo-potential calculations as performed by Pandey, Platzman, and Eisenberger²⁶ apparently have been overestimated. Therefore, only a few band-structure calculations of $S(\mathbf{q}, \omega)$ exist,²⁷⁻²⁹ where only the calculation of Taut and Hanke²⁹ on Be has been extended far into the intermediate momentum-transfer regime, $q > q_c$, although by neglecting local-field effects. But in spite of the fact that this calculation is strictly within RPA and takes into account only a final-state independent lifetime, it has yielded a fine structure of $S(\mathbf{q}, \omega)$, the main feature of which is a double peak with a dispersion, which reproduces the x-ray results of Miliotis³⁰ nicely. Therefore, it cannot be ruled out that, at least in some cases, the fine structure of $S(\mathbf{q}, \omega)$ is due to special features of the band structure. This argument gets support by the theoretical estimation of ZBCS's in Al by Sturm and Oliveira.⁶

Faced with this rather confusing situation, both with respect to experimental and theoretical results, new experiments seem to be indispensable, where these experiments have to fulfill the following requirements.

(i) Sufficient energy resolution, statistical accuracy and signal-to-background ratio, in order to reveal the fine structure of $S(\mathbf{q}, \omega)$ on a 1-eV scale and to see possible oscillations of a few percent of maximum intensity.

(ii) Only small influence of multiscattering events on the final result, in order to get unambiguously the full shape of $S(\mathbf{q}, \omega)$.

(iii) Well-defined direction of the scattering vector \mathbf{q} with respect to a single-crystal scatterer, in order to make possible a better distinction of crystal lattice effects from correlation and lifetime effects.

According to our introductory remarks to the previous experimental situation, only inelastic x-ray scattering experiments utilizing the potentialities of synchrotron x-ray radiation seem to satisfy all the above-mentioned requirements in a wide range of momentum transfer, mainly for $q > q_c$. Therefore, after a short survey in Sec. II of all re-

lations which are necessary for understanding both the experimental arrangements and the theoretical interpretation of the experimental results, the setup at the DORIS storage ring is described in Sec. III in some detail. In Sec. IV the results of the inelastic x-ray scattering measurements on Li single crystals are presented, where emphasis is on the presentation of the $q > q_c$ experiments.

It may have become evident in our introductory remarks to the theoretical situation that any attempt to interpret new experimental results of $S(\mathbf{q}, \omega)$ has to take into account exchange and correlation effects (deviations from RPA) just as the finite lifetime of quasiparticles, and, last not least, also crystal lattice effects in an appropriate manner. This is done in Sec. V, where the experimental results are confronted with calculations for the inhomogeneous case by means of a local pseudopotential going beyond RPA. Finally, Sec. VI contains concluding remarks.

II. BASIC RELATIONS

Within the limits of first-order perturbation theory, the double differential cross section $d^2\sigma/d\omega d\Omega$ for inelastic x-ray scattering is directly connected with the dynamic structure factor $S(\mathbf{q}, \omega)$ by the following relation:³¹

$$d^2\sigma/d\Omega d\omega = (\mathbf{e}_0 \cdot \mathbf{e}')^2 r_0^2 (\omega' / \omega_0) S(\mathbf{q}, \omega), \quad (1)$$

where $\hbar\omega_0$ and $\hbar\omega'$ are the energies, \mathbf{e}_0 and \mathbf{e}' are the polarization vectors of the incident and the scattered x-ray photons, respectively, $\hbar\omega$ is the energy transferred to the scattering system, \mathbf{q} is the transferred momentum, and r_0 is the classical electron radius.

The dynamic structure factor $S(\mathbf{q}, \omega)$ is related to the dielectric response function $\epsilon^{-1}(\mathbf{q}, \omega)$ via the fluctuation-dissipation theorem:³²

$$S(\mathbf{q}, \omega) = -(\hbar q^2 / 4\pi^2 e^2 n) \text{Im} \epsilon^{-1}(\mathbf{q}, \omega), \quad (2)$$

where n is the electron density and $\epsilon^{-1}(\mathbf{q}, \omega)$ is formally defined in terms of the response of the electron system to an external longitudinal potential $\phi_{\text{ext}}(\mathbf{q}, \omega)$, i.e.,

$$\epsilon^{-1}(\mathbf{q}, \omega) \equiv \phi_{\text{tot}}(\mathbf{q}, \omega) / \phi_{\text{ext}}(\mathbf{q}, \omega). \quad (3)$$

It is the aim of the rest of this section to provide all basic relations which are used in the model calculations presented in Sec. V in order not to complicate this chapter with definitions and formal background. It should already be stressed that these basic relations do not claim to be the formal framework of a first-principles calculation. These relations are, on the contrary, a sequence of steps of approximations to the response $\epsilon^{-1}(\mathbf{q}, \omega)$ of metal valence electrons and have been already utilized more or less separately by several authors for interpreting $S(\mathbf{q}, \omega)$ measurements.

The first step is to reduce the ion action on the electrons to a uniform positive background by using the jellium model, where the electron-electron interaction is taken into account within the limits of the random-phase approximation (RPA), this means by complete neglect of exchange and correlation. In this case, $\epsilon(\mathbf{q}, \omega)$ is the well-known Lindhard's longitudinal dielectric function³³ the analytic expression of which is the result of the following

momentum space integration:

$$\epsilon^L(\mathbf{q}, \omega) = 1 - \lim_{\eta \rightarrow 0} \frac{e^2 V}{\hbar q^2 \pi} \int d\mathbf{p} \frac{f_0(\mathbf{p} + \mathbf{q}) - f_0(\mathbf{p})}{E(\mathbf{p} + \mathbf{q}) - E(\mathbf{p}) - \hbar\omega + i\eta}, \quad (4)$$

where $E(\mathbf{p})$ and $f_0(\mathbf{p})$ are the energy and the occupation number, respectively, of the momentum eigenstate $|\mathbf{p}\rangle$.

For $q < q_c$, $S(\mathbf{q}, \omega)$ according to Eq. (4) is dominated by the plasmon resonance, the energetic position $\omega(q)$ of which is determined by the poles of $\epsilon^{-1}(\mathbf{q}, \omega)$, approximately given by the well-known RPA plasmon dispersion relation:

$$\omega(q)^2 = \omega_p^2 + \alpha q^2 + \dots, \quad \alpha = 3v_F^2/5, \quad (5)$$

where $\omega_p = 4\pi n e^2 / m$, and v_F is the Fermi velocity. The plasmon cutoff vector q_c is defined as the minimum plasmon wave vector, which makes possible the transfer of the plasmon energy to one electron-hole pair. Beyond q_c , within the limits of the RPA, the plasmon is no longer a well-defined elementary excitation of the electron liquid, since the plasmon will decay very fast into an electron-hole pair, appearing thus strongly damped. Therefore, within the limits of RPA, $S(\mathbf{q}, \omega)$ is dominated by electron-hole pair excitation for $q > q_c$.

The second step to an appropriate description of metal valence electrons can be done by introducing the finite lifetime of the single particle states following the idea of Mukhopadhyay, Kalia, and Singwi.¹³ As has been shown by Rahman and Vignale¹⁶ this can be done without violating the f sum rule by replacing $E(\mathbf{p})$ and $E(\mathbf{p} + \mathbf{q})$ in Eq. (4) by $E(\mathbf{p}) + i\Gamma(\mathbf{p})$ and $E(\mathbf{p} + \mathbf{q}) + i\Gamma(\mathbf{p} + \mathbf{q})$, respectively, where $\Gamma(\mathbf{p})$ is the momentum-state-dependent inverse lifetime. Within the framework of the approximation, as introduced by Singwi, Tosi, Land, and Sjölander,^{34,35} the imaginary part of the electron self-energy $\Sigma_I(p, E(p))$ serves as the inverse lifetime. A useful approximation to Σ_I , which is strictly a RPA, was given by Quinn³⁶ and will be used in the numerical calculations of Sec. V, in order to get a fitting parameter free estimation of the momentum-state-dependent inverse lifetime.

As pointed out both by Niklasson, Sjölander, and Yoshida¹⁷ and by Rahman and Vignale,¹⁶ we have to distinguish two very different ranges, when plotting Γ of an electron liquid against the quasiparticle momentum p (see Fig. 1). For $p < p_0$, Γ is much smaller than for $p > p_0$, where p_0 is the minimum quasiparticle momentum, which makes possible the decay of the quasiparticle state into a plasmon, i.e.,

$$\hbar\omega(q_c) = (\hbar^2/2m)(p_0^2 - p_F^2), \quad (6)$$

with the plasmon energy $\hbar\omega(q_c)$ at the plasmon cutoff vector and the Fermi momentum p_F .

This steplike behavior of Γ at p_0 can be understood easily within the limits of the RPA, since for $q < q_c$, the excitation of a plasmon has a much higher probability than the excitation of an electron hole pair. On the other hand, it must be conceded that this way of introducing lifetime effects into a calculation of $S(\mathbf{q}, \omega)$ violates the continuity equation, as first pointed out by Mermin³⁷ for the case of a momentum-independent lifetime, and later in

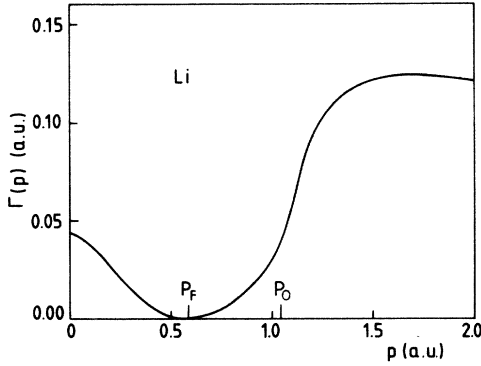


FIG. 1. Inverse quasiparticle lifetime Γ as a function of momentum p calculated for the electron density of Li according to Ref. 36; p_F is the Fermi momentum. For $p > p_0$ quasiparticles can decay by emitting a plasmon.

Ref. 20 for momentum-dependent damping. But it has been shown in Ref. 17 by means of a model calculation that a particle conserving scheme does not vary the essentials of the nonconserving one. Nevertheless, this point seems to be the most severe shortcoming of our model calculation in Sec. V, since it is difficult to estimate quantitatively its influence on the final result.

The third step in our approach has to introduce exchange and correlation into the jellium model. As first proposed by Hubbard,³⁸ this can be done approximately by means of a so-called local-field factor $G(q, \omega)$, which

$$T_{\mathbf{g}\mathbf{g}'} = \frac{4\pi e^2}{(\mathbf{q} + \mathbf{g})^2} \lim_{\eta \rightarrow 0} \sum_{\mathbf{k}, l} \frac{\langle \mathbf{k}l | e^{-i(\mathbf{q} + \mathbf{g}) \cdot \mathbf{r}} | \mathbf{k}'l' \rangle \langle \mathbf{k}'l' | e^{i(\mathbf{q} + \mathbf{g}') \cdot \mathbf{r}} | \mathbf{k}l \rangle}{\hbar\omega + E(\mathbf{k}, l) - E(\mathbf{k}', l') + i\eta} [f_0(\mathbf{k}', l') - f_0(\mathbf{k}, l)], \quad (9)$$

where the electron states are represented by one-electron Bloch states with reduced wave vector \mathbf{k} , band index l , and energy $E(\mathbf{k}, l)$; $f_0(\mathbf{k}, l)$ is the occupation number of the state $|\mathbf{k}l\rangle$. If one neglects all microscopic local-field effects, which are introduced by the periodicity of the solid, the dielectric matrix $\delta_{\mathbf{g}\mathbf{g}'} - T_{\mathbf{g}\mathbf{g}'}$ of Eq. (8) is simply reduced to its first diagonal element $\delta_{00} - T_{00}$, so that the well-known Ehrenreich-Cohen dielectric function comes out, i.e.,

$$\epsilon(\mathbf{q}, \omega) = 1 + \lim_{\eta \rightarrow 0} \frac{4\pi e^2}{q^2} \sum_{\mathbf{k}, l} \frac{|\langle \mathbf{k}'l' | e^{i\mathbf{q} \cdot \mathbf{r}} | \mathbf{k}l \rangle|^2}{\hbar\omega + E(\mathbf{k}, l) - E(\mathbf{k}', l') + i\eta} \times [f_0(\mathbf{k}', l') - f_0(\mathbf{k}, l)]. \quad (10)$$

As first pointed out by Foo and Hopfield,⁷ one prominent contribution in monovalent simple metals such as Li, possibly the most important contribution, of the periodic lattice to the fine structure of $S(\mathbf{q}, \omega)$ arises for those transitions $|\mathbf{k}, l\rangle \rightarrow |\mathbf{k}', l'\rangle$ in Eq. (10), which, for a given momentum transfer q , begin or end up on a Bragg plane in the extended-zone scheme, where the Bragg plane is defined by

allows the calculation of a local-field-corrected dielectric function $\epsilon(\mathbf{q}, \omega)$, using the RPA longitudinal dielectric function $\epsilon^L(\mathbf{q}, \omega)$ of Eq. (4), via the following relation:

$$\epsilon(\mathbf{q}, \omega) = 1 + \frac{\epsilon^L(\mathbf{q}, \omega) - 1}{1 - G(\mathbf{q}, \omega)[\epsilon^L(\mathbf{q}, \omega) - 1]}. \quad (7)$$

In Sec. V we will use the static approximation $G(\mathbf{q})$ of the local-field factor $G(\mathbf{q}, \omega)$, and we will utilize the analytic expression for $G(\mathbf{q})$, as given by Ichimaru and Utsumi.³⁹ This analytic form of $G(\mathbf{q})$ closely simulates both the results of the microscopic theory⁴⁰ and Monte Carlo calculations.⁴¹

The last step of our approach is the appropriate inclusion of electron-ion interaction in a crystalline solid. According to the local-field dielectric theory of Wisner,⁴² Saslow and Reiter⁴³ have introduced the effects of band structure into the theory of characteristic energy losses of electrons in periodic solids. These theoretical considerations have been applied to inelastic x-ray scattering of solids by Platzman and Wolff,⁴⁴ ending up with an expression for the dynamic structure factor, where one has to replace $\epsilon^{-1}(\mathbf{q}, \omega)$ in Eq. (2) by the first diagonal element of the inverse dielectric matrix as introduced by Wisner,⁴² i.e.,

$$\epsilon^{-1}(\mathbf{q}, \omega) = (\delta_{\mathbf{g}\mathbf{g}'} + T_{\mathbf{g}\mathbf{g}'})^{-1}_{00}. \quad (8)$$

\mathbf{g} and \mathbf{g}' are reciprocal-lattice vectors.

Within the limits of the self-consistent-field theory,⁴⁵ which is equivalent to RPA, the matrix $T_{\mathbf{g}\mathbf{g}'}$ reads as follows:

$$\mathbf{k} \cdot \mathbf{g} = g^2/2, \quad (11)$$

provided all these transitions will lead to the same energy transfer $\hbar\omega$ in the empty lattice. If one is guided by the empty lattice model, this will happen, if \mathbf{q} is parallel to the corresponding reciprocal lattice vector of the Bragg plane. Since states on such a Bragg plane belonging to different bands l and l' are degenerated in the empty lattice, a gap in the combined density of states can arise (accompanied by peaks on both sides of the gap) when the periodic potential is switched on. According to Eq. (10), this structure of the combined density of states is repeated in the imaginary part $\epsilon_2(\mathbf{q}, \omega)$ of the dielectric function as shown in Fig. 2. Other transitions can fill up this gap to a certain extent, but nevertheless this gap (or local minimum) of ϵ_2 can produce an additional zero of the real part $\epsilon_1(\mathbf{q}, \omega)$ of the dielectric function via the Kramers-Kronig relation. Within the limits of the RPA, such a behavior of ϵ_1 and ϵ_2 should give rise to a very strong peak in $-\text{Im}\epsilon^{-1}(\mathbf{q}, \omega) = \epsilon_2/(\epsilon_1^2 + \epsilon_2^2)$, which can be interpreted as a new collective mode, the so-called zone-boundary collective state (ZBCS).⁷

But even if the local minimum of ϵ_2 is not sufficiently strong to produce an additional zero of ϵ_1 , the structure of ϵ_1 in the neighborhood of the ϵ_2 minimum can cause a

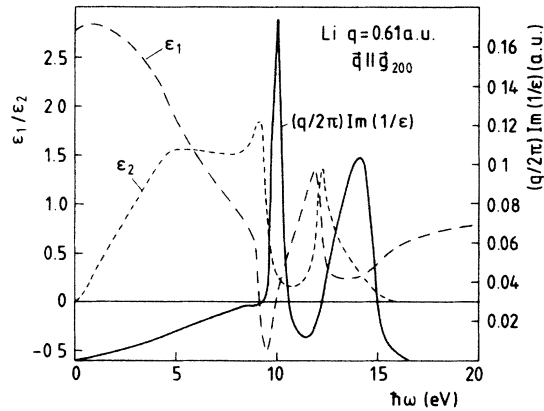


FIG. 2. Real part $\epsilon_1(\mathbf{q}, \omega)$ (dashed-dotted line), imaginary part $\epsilon_2(\mathbf{q}, \omega)$ (dashed line) of the dielectric function $\epsilon(\mathbf{q}, \omega)$, and the imaginary part of the reciprocal dielectric function $\text{Im}(1/\epsilon)$ (solid line) calculated for a two-band model of Li (only $\mathbf{g}=0$, \mathbf{g}_{200} , and $\mathbf{g}_{\bar{2}00}$ are included, $\mathbf{q} \parallel [100]$; $q=0.61$ a.u.).

prominent structure in $\text{Im}\epsilon^{-1}$, namely a maximum on the low ω side followed by a minimum, as plotted in Fig. 3. According to Eq. (11), the dispersion of both the ZBCS's and the structure, which arises as a consequence of the ϵ_2 minimum, will follow roughly

$$\omega(q) = \frac{q}{2}(g - q), \quad (12)$$

if the final states are on the g th Bragg plane, and

$$\omega(q) = \frac{q}{2}(g + q), \quad (13)$$

if the initial states are on the g th Bragg plane, provided that in both cases $\mathbf{g} \parallel \mathbf{q}$. This leads in the first case to a weak dispersion, whereas the dispersion in the second case is strong, roughly quadratic in q .

As long as transitions to states on Bragg planes with $\mathbf{g} \parallel \mathbf{q}$ are the most prominent contributions to the combined density of states, so that there exists only minor destructive interference of all other equivalent reciprocal lattice vectors, it will be justified to calculate $\epsilon(\mathbf{q}, \omega)$ according to Eq. (10) within the limits of a two-band model by

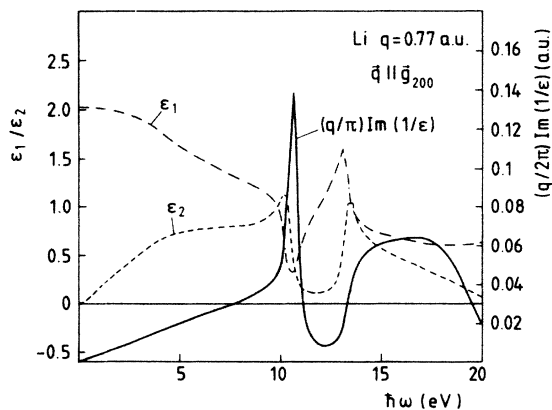


FIG. 3. Same as Fig. 2, but for $q=0.77$ a.u.

representing the lattice periodicity, besides $\mathbf{g}=0$, only by two reciprocal lattice vectors \mathbf{g} and $-\mathbf{g}$, which are parallel to \mathbf{q} and have a nonvanishing Fourier component $V_{\mathbf{g}}$ of the lattice potential. As shown by Sturm and Oliveira,⁶ these two-band calculations can be performed analytically. Figures 2 and 3 were thus obtained. The results of this approach can serve as a valuable guide to a full physical understanding of the lattice induced structures of $S(\mathbf{q}, \omega)$, even though these calculations often will overestimate the zone-boundary-influenced structures.

Since the dielectric function of Eq. (10) is the result of a mean-field theory of the periodic lattice, equivalent to the RPA of the jellium, it seems to be justified for a model calculation to introduce both lifetime effects and effects of exchange and correlation into the dielectric response of a crystalline solid in the same manner as already done within the framework of the jellium model. Therefore, in order to approximately take into account the lifetime of quasiparticle states, we will replace in Eq. (10) $E(\mathbf{k}, l)$ and $E(\mathbf{k}, l')$ by $E(\mathbf{k}, l) + i\Gamma(p)$ and $E(\mathbf{k}', l') + i\Gamma(p')$, respectively, where

$$p = 2mE^{1/2}(\mathbf{k}, l); \quad p' = 2mE^{1/2}(\mathbf{k}', l'), \quad (14)$$

and $\Gamma(p)$ is calculated for the homogeneous case.

This introduction of lifetime is by far not done in a self-consistent way, since the free-electron self-energy is used for calculating $\Gamma(p)$ instead of introducing lattice effects also at this point. But this procedure seems to be justified, since it will turn out that, in the case of Li, the overall behavior of $\epsilon(\mathbf{q}, \omega)$ is nearly free-electron-like, in spite of some remarkable lattice effects. The inclusion of exchange and correlation for the periodic solid has been done in the same manner as for the homogeneous case [i.e., by means of Eq. (7), where $\epsilon^L(\mathbf{q}, \omega)$ is now the dielectric function of Eq. (10)], by utilizing again the static approximation $G(q)$ of the local-field factor $G(\mathbf{q}, \omega)$, as calculated for free electrons.

III. EXPERIMENTAL SETUP AND DATA PROCESSING

The double differential inelastic scattering cross section was measured by use of a spherically bent Si-crystal spectrometer in nearly Bragg back-reflection geometry for the energy analysis of the scattered radiation, as sketched in Fig. 4, in connection with a double-crystal monochromator, which provides monochromatic photons from the white synchrotron radiation beam of DORIS II. The spectral analysis of the scattered radiation was performed by holding the Bragg angle θ_{BA} of the analyzer fixed and by varying the primary energy. One part of the following experimental results (those for $0.6 < q/q_c < 1.67$) was obtained with that one performance of the spectrometer, which has been described in detail elsewhere.⁴⁶ Si(400) double-crystal monochromator with independent two-crystal setting,⁴⁷ which provides $\approx 1 \times 10^9$ photons s^{-1} of $E_0 = 5.95$ keV within a relative bandpass $\Delta E/E_0 = 2 \times 10^{-4}$ at the scattering sample into an illuminated area of 0.5 cm². In connection with a Si(333) spherically bent crystal analyzer, one gets an overall energy resolution of the spectra [measured as the full width at half max-

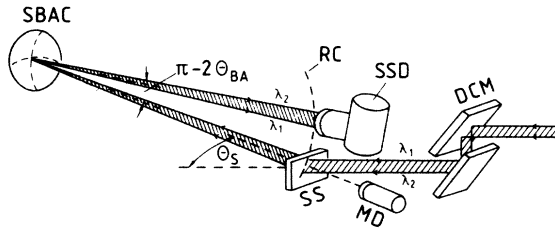


FIG. 4. Experimental setup: DCM is the double-crystal monochromator; SS is the scattering sample; SBAC is the spherically bent analyzer crystal; RC is the Rowland circle; SSD is the solid-state detector; and MD is the monitor detector. The dispersion compensating geometry is sketched. The wavelengths λ_1 and λ_2 at the upper and lower limit of the DCM bandpass are Bragg reflected simultaneously by the SBAC.

imum (FWHM) of the Rayleigh line] of 1.35 eV.

For the other part of the experimental results, a modification of the setup was utilized, which provides a much higher photon flux at the scattering sample but leaves the overall energy resolution unchanged or even improved. In this version the monochromator consists of Ge(220) crystals providing $\approx 6 \times 10^9$ photons $^{-1}$ of $E_0 = 5.95$ keV within a relative bandwidth $\Delta E/E_0 = 5 \times 10^{-4}$ into an illuminated area on the sample which has a vertical height of $b = 5$ mm and a horizontal width of 10 mm, both limited by a corresponding diaphragm, the source-sample distance was $L = 25$ m.

Since the vertical height c of the source is only ≈ 1 mm, and thus much smaller than b , there exists a spectral distribution across the vertical dimension z of the illuminat-

ed area at the sample with longer wavelengths at the top and shorter wavelengths at the bottom, as sketched in Fig. 4. By an appropriate choice of the Bragg angle θ_{BM} of the monochromator one can arrange things so that, according to the Rowland geometry of the spherically bent analyzer, the whole wavelength distribution across the vertical dimension z is Bragg reflected simultaneously by the analyzer. It turns out that in this dispersion compensating case, which will be published in greater detail elsewhere,⁴⁸ the overall energy resolution of the experiment is in a good approximation given by

$$\Delta E/E = (c/L)\cot\theta_{BM}, \quad (15)$$

provided that the Darwin width of both the monochromator and the analyzer are of less importance.

Thus one ends up with an overall energy resolution of the experiment of 1.0 eV. The diameter $D = 4$ cm of the spherically bent analyzer crystal together with the sample to analyzer crystal distance $R = 80$ cm defines an error $\Delta q = \pm 0.03$ a.u. of momentum transfer, nearly independent of the scattering angle within the range used. The count rate in the peak of the inelastically scattered spectrum was ≈ 80 Hz for $q = 0.92$ a.u. when the source data were 3.7 GeV and 50 mA. The background, as measured at the high-energy side of the Rayleigh line, was less than 0.2 Hz under the above conditions, so that the peak signal to background ratio was better than 400. In every case $\approx 10^4$ counts were collected in the inelastic peak, which is equivalent to $\approx 1\%$ statistical accuracy.

The Li single crystal (99.9% Li, grown by a modified Bridgeman technique), a plate of 3 mm thickness, which contains the [100], [110], and [111] direction in its surface, was etched to metallic luster before putting it into

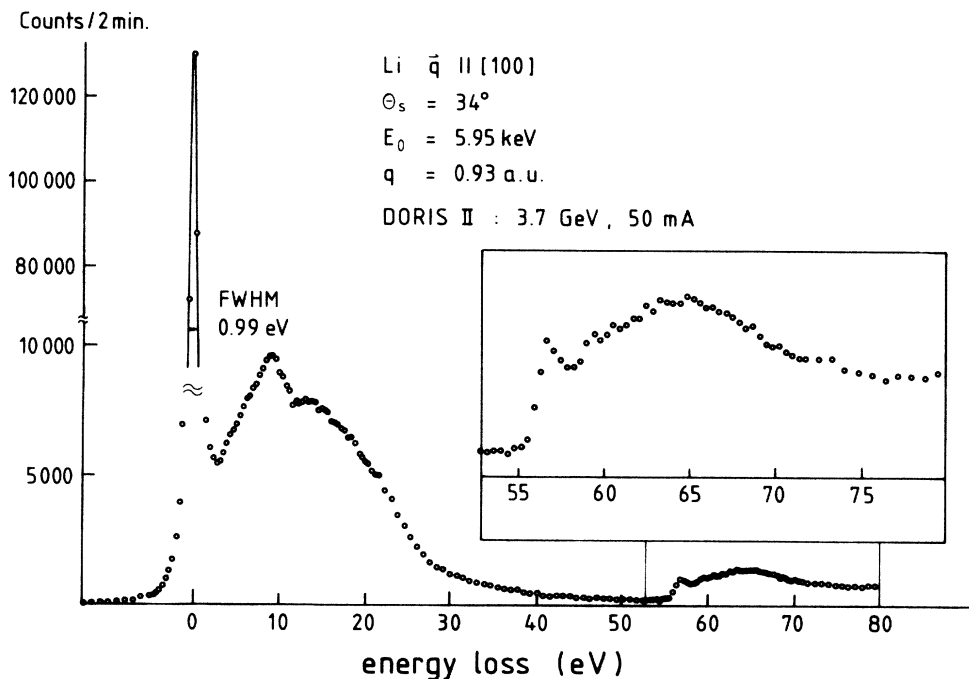


FIG. 5. Rough experimental data for $q \parallel [100]$; $q = 0.93$ a.u. In the insert a magnified detail around the K -edge structure is displayed.

the evacuated (10^{-3} Torr) scattering chamber. After the measurement the metallic luster had survived.

Both, the monitor detector, which looks upon the irradiated part of the scattering sample, and the detector, which measured the radiation Bragg reflected by the analyzer, were solid-state detectors. By this means the contamination of the monochromatized beam with higher harmonics was controlled completely.

As an example of the rough experimental data, the measurement with $q \parallel [100]$; $q=0.93$ a.u. is displayed in Fig. 5. The spectrum consists of three well-separated sections: (i) the quasielastically scattered Rayleigh line, the energetic width of which is a measure of the total energy resolution; (ii) the contribution of the Li valence electrons to inelastic scattering (in Fig. 5 between 0 and ≈ 50 eV), this is the part we are mainly interested in; (iii) the contribution of the core electrons to inelastic scattering with an edgelike onset at the $1s$ binding energy of 55 eV.

As already pointed out in Ref. 12, multiple scattering had no significant influence on our spectra. This was tested by measuring the same spectrum with $q \parallel [100]$, $q=0.77$ using a 2- and a 6-mm-thick sample, respectively. After data reduction as described below, the spectra were identical within statistical accuracy. This is also true for the long tail at higher values of energy loss.

The experimental data were processed as follows.

(i) A linear background as determined by the count rate on the high-energy side of the Rayleigh line was subtracted.

(ii) Since the count rate of the detector behind the analyzing crystal is normalized to the count rate of the monitor detector, the data have not to be corrected for the weak-energy dependence of both the scattering cross sec-

tion [see Eq. (1)] and the spectral transmission of the whole spectrometer (mainly determined by the energy dependence of the monochromator reflectivity).

(iii) The Rayleigh line was removed from the data assuming it to be symmetric and superimposed by the inelastically scattered part of the spectrum only in its low-energy half. Since the Rayleigh line is 7 to 12 times higher than the peak of the inelastic spectrum, this procedure leads to less reliability of the inelastic spectrum in its initial part between 0 and 2 eV energy loss.

(iv) For the sake of comparison with theoretical calculations the experimental values of the dynamic structure factor were brought to an absolute scale by means of (a slightly modified) f sum rule:

$$\int_0^{\infty(\omega_e)} S(\mathbf{q}, \omega) \omega d\omega = f(q) \hbar^2 q^2 / 2m, \quad (16)$$

where the factor $f(q)$ takes into account the core polarizability, as described in more detail in Sec. V. The choice of the upper limit ω_e in Eq. (16) is not without some arbitrariness since at all measurements with $q > q_c$, the low-energy side of the spectra did not reach the background as measured on the high-energy side of the Rayleigh line. Because the origin of this very long tail of the spectra could be either transitions from deep-lying plasmonlike states of the valence electrons predicted by Lundquist⁴⁹ or anomalous contribution of core electrons, as presumed by Sturm⁵⁰ (multiple scattering as the origin of this tail was ruled out experimentally), we decided to fix ω_e on the high-energy-transfer side of the spectrum at a position, where, after background subtraction, the counting rate was 2% of the peak rate. If this value is not reached, due to the onset of the core contribution, we made a linear ex-

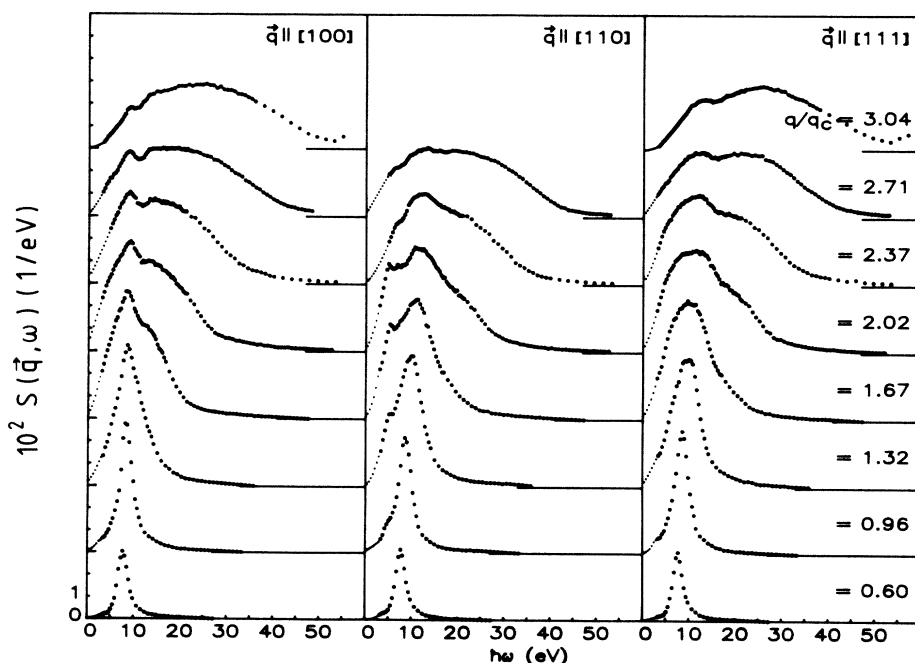


FIG. 6. Survey of all experimental results after data processing and normalization. The small dots in the region of low-energy transfer ω represent that part of the spectra, which is less reliable because of heavy superposition by the Rayleigh line in the rough data.

trapolation of the decreasing part of the spectrum till to the 2% position. Because of the uncertain origin of the low-energy tail of the spectra, this point will need further attention, especially, if the static structure factor $S(q)$ should be obtained by integrating the normalized $S(q, \omega)$ spectra.

IV. EXPERIMENTAL RESULTS

Figure 6 is a survey of all experimental results obtained for Li. The transferred momentum q is given in units of $q_c = 0.46$ a.u., the transferred energy $\hbar\omega$ in eV, and $S(q, \omega)$ in $(\text{eV})^{-1}$. For $q < q_c$, the spectra are single peaked resembling the well-known RPA result of a homogeneous electron system, where plasmon excitation is the most prominent contribution to the dynamic structure factor. In Fig. 7, the position of these peaks are given in an ω - q plot together with the RPA plasmon dispersion of a homogeneous system with the electron density of Li, according to Eq. (5). The plasmon-peak dispersion seems to exhibit a small orientation dependence, where the dispersion coefficient α [see for definition Eq. (5)] follows

$$\alpha_{\text{RPA}} > \alpha_{110} \approx \alpha_{111} > \alpha_{100}. \quad (17)$$

But the number of measurements with $q < q_c$ is overly small, and the error bar Δq of the momentum transfer is overly large to get reliable quantitative results for the orientation dependence of α . The same is true with the plasmon linewidth. As already mentioned, the emphasis of these results is on the region $q > q_c$. The results of an investigation of the plasmon resonance in single-crystal Li with better q resolution will be given elsewhere.

The deviation of the experimental plasmon-peak position from the homogeneous RPA result, as shown in Fig. 7, is well known from electron-energy-loss measurements⁵¹ and is due to intraband transitions, as pointed out by Paasch.⁵² For $q > q_c$ the spectra become much broader

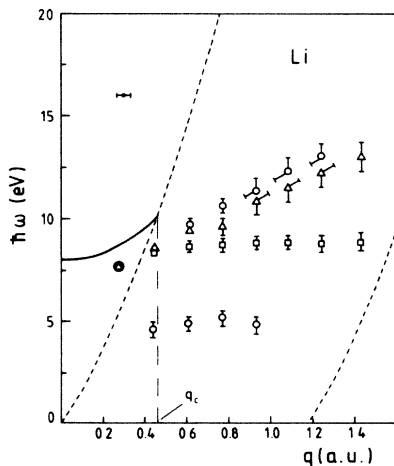


FIG. 7. ω - q plot of experimental peak positions: squares, first peak of the [100] spectra; circles, first and second peak, respectively, of the [110] spectra; triangles, first peak of the [111] spectra; solid line, homogeneous RPA plasmon dispersion; and dotted lines enclose the region of single-particle excitation.

and exhibit a fine structure which turns out to be strongly orientation dependent. This can be seen in particular, when looking at the position of the first peak both in the [100] and [111] spectra and of the first two peaks in the [110] spectra for $q > q_c$ as plotted in Fig. 7. The peak near 5 eV is present only in the [110] spectra within a limited range of q/q_c . Its energetic position is not far from the empty lattice position $\omega(q)$ of the g_{110} excitation gap for $q=0.75$ as given by Eq. (12), namely $\omega(q)=5.9$ eV. Thus it seems reasonable to attribute this peak to lattice effects and to think of structures, which are due to the band gap across the (110) Bragg plane perpendicular to q , and which are discussed in Sec. II in terms of ZBCS's. Since ZBCS's in the strict sense of a new collective mode are presented in Sec. II only within the limits of a two-band model, one has to perform band structure calculations of $S(q, \omega)$ by at least taking into account the influence of all equivalent reciprocal lattice vectors of (110) type via their potential coefficients in order to rule out complete destructive interference of the (110)-type reciprocal lattice vectors, which are not parallel to q , on the excitation gap and the corresponding structure of $S(q, \omega)$. These calculations are presented in Sec. V.

The peaks in the range between 9 and 13 eV exhibit a remarkable orientation dependence not only with respect to their position but also as far as the "peak-width" is concerned, where the peak width is represented in Fig. 7 by means of the error bars on their energy position. Whereas the peaks in the [110] and [111] spectra are broad and positioned from 10 to 13 eV with a weak dispersion, the peak in the [100] spectra is sharp and positioned near 9 eV with nearly no dispersion. Moreover, only for $q \parallel [100]$ and by no means for $q \parallel [110]$ or [111], there exists a Bragg plane perpendicular to q , which gives a reasonable position of the corresponding excitation gap and which is known from first-principles band-structure calculation⁵³ to exhibit a strong band gap over a large area within the extended-zone scheme. The empty lattice position $\omega(q)$ of the corresponding g_{200} excitation gap for $q=0.75$ is 11.8 eV, which, of course, seems to be overly far away from 9 eV. But taking into account that, according to Fig. 2, the peak of $S(q, \omega)$ corresponding to such an excitation gap is at the lower edge of the gap and taking into consideration that the band gap of first-principles band calculation would produce an excitation gap at a position nearly 2 eV lower than the empty lattice position due to exchange-induced band narrowing, it seems again reasonable to attribute the peak around 9 eV of the [100] spectra to lattice effects which are due to the band gap across the (200) Bragg plane. Again it is indispensable to support this assumption by means of band-structure calculation, which take into account the influence of all other equivalent reciprocal lattice vectors of the (200) type and to prove, whether or not this influence is destructive.

For the corresponding broad peaks in the [110] and [111] spectra, no crystal-lattice-induced origin is suggested by consideration given so far. Therefore it remains the task of the following model calculations of Sec. V to look for their physical reason. The same is true with the broad peak in the spectra of all three directions, which exhibit a

very strong dispersion and which starts to develop from a shoulder beginning at $q/q_c=2.02$. Contrarily, the position and the depth of the dip between the weak (or zero) dispersive peak between 9 and 13 eV on one side and the broad and strong dispersive peak on the other side reflects an orientation dependence, which is strongly correlated with the orientation dependence of the weak dispersive peak.

Therefore it remains for the present an open question to what extent this dip is crystal lattice induced or a more common feature of the strongly correlated electron system as proposed in Refs. 17 and 18. Thus, this problem can also be solved, if at all, by means of calculation, which include crystal-lattice as well as momentum-dependent lifetimes and local field as proposed in Sec. II. These calculations are presented in Sec. V.

V. COMPARISON WITH CALCULATIONS AND DISCUSSION

It is the aim of this section to present calculations of $S(\mathbf{q},\omega)$ that are not first principles in the strict sense of this word, but consist of a stepwise approach as sketched in Sec. II. But nevertheless these calculations are much more than a fitting procedure, since every step to the final result consists of a correction to the preceding result based on fitting-parameter free calculations. This is true with respect to the introduction of band structure, momentum-dependent lifetime, local-field correction, and core polarizability. Even the small deviation of only one local pseudopotential coefficient from its theoretical value was not fitted to the above experimental results but chosen to fit better first-principles band-structure calculation.

Nevertheless each correcting step of the following model calculation is in itself an approximation, since it always contains assumptions which should be listed first comprehensively.

(i) The introduction of band structure is a simple local pseudopotential approach, which neglects core orthogonalization. Also the off-diagonal terms of the dielectric matrix, as introduced by the periodic lattice potential, have not been taken into account.

(ii) The momentum-dependent lifetime has been introduced on a strictly RPA base. The corresponding real part of the self-energy has been neglected.

(iii) Local-field corrections have been done in the static approximation.

(iv) The core polarizability has been considered simply by using the free-ion polarizability.

In the following, the result of each step is displayed separately to elucidate the extent of the contribution of each correcting step to $S(\mathbf{q},\omega)$.

As already pointed out in Sec. II, the first step to a full understanding of the dynamic response of an interacting electron system of a simple metal is to treat it as a homogeneous electron liquid in RPA, or to calculate the dynamic dielectric properties by including band-structure effects within the limits of the self-consistent field (SCF) theory.⁴⁵ As an example of such a calculation, the homogeneous RPA $S(\mathbf{q},\omega)$ and the band structure including

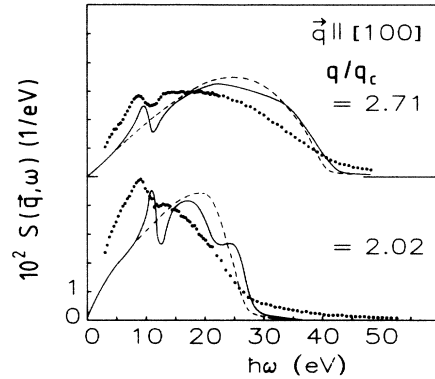


FIG. 8. Calculated RPA $S(\mathbf{q},\omega)$ for $\mathbf{q}||[100]$; $q/q_c=2.02$ and $q/q_c=2.71$; dashed line, homogeneous electron liquid; solid line, pseudopotential band structure; and dots, experimental values.

SCF $S(\mathbf{q},\omega)$ is shown for Li; $\mathbf{q}||[100]$ with $q/q_c=2.02$ and $q/q_c=2.71$, together with the experimental result in Fig. 8. In this and all following calculations, band-structure effects are introduced by using a local pseudopotential with the following Fourier coefficients (in a.u.): $V_{110}=0.05$, $V_{200}=0.055$, $V_{211}=0.008$, $V_{220}=-0.005$, $V_{310}=-0.007$, $V_{222}=-0.005$, $V_{321}=-0.002$, $V_{400}=0.001$, $V_{330}=0.003$, $V_{420}=0.003$, $V_{332}=0.002$, $V_{422}=0.001$, and by taking into account 44 reciprocal lattice vectors, when diagonalizing is performed. Core orthogonalization was neglected, when calculating wave functions for the matrix elements of Eq. (10). The potential coefficients are chosen according to the Li form factors, as given by Heine and Abarenkov.⁵⁴ Only the V_{200} coefficient had to be changed from 0.04 to 0.055 in order to reproduce the correct order of energy eigenvalues at the H point, as given by more sophisticated band-structure calculations on Li, e.g., by Bross and Bohn.⁵³ This point will be stressed once more at the end of this section. These and all following calculated spectra were convoluted with the experimental resolution.

It is evident that the homogeneous RPA result is far from being in agreement with the experimental data. The introduction of the band structure within the SCF scheme does not improve the overall agreement with experiment that much. But the most prominent peak of the experimental spectra between 9 and 10 eV, and the accompanying dip near 12 eV, seem to be consistent with a corresponding peak and dip in the SCF calculations, even though the peak position of the calculated curves is somewhat shifted to higher energy losses. It can easily be proved that this structure in the SCF calculations for $\mathbf{q}||[100]$ is due to the band gap across the (200) Bragg plane perpendicular to \mathbf{q} [see also statement (iii) of this section]. Therefore it seems to be justified to attribute the experimental peaks between 9 and 10 eV, together with the dip at 12 eV, to this band gap and to speak of a ZBCS-like structure in the sense of the consideration as given in Sec. II demonstrated by Figs. 2 and 3. It is of importance for this interpretation of the peaks in the [100] spectra that the ZBCS-like structure of the two-

band model proves not to be destroyed in the complete band-structure calculations by interference with other equivalent Bragg planes of (200) type. This point was treated in detail in Ref. 6, where conditions are given for a nondestructive cooperation of Bragg planes of the same type. The same is true, when comparing experimental [110] results with corresponding SCF band-structure calculations. The peak structure at 5 eV of the experiment can be clearly attributed to the band gap across the (110) Bragg plane.

As already pointed out, a second step to a proper treatment of metal valence electrons consists in the inclusion of lifetime effects in a manner described in Sec. II. By using the approximation for $\Sigma_I(p)$ as given by Quinn,³⁶ $\Gamma(p) = |\Sigma_I(p)|$ was calculated for Li (see Fig. 1) and was introduced into the RPA relations for $S(\mathbf{q}, \omega)$ in the f sum rule conserving way, proposed by Rahman and Vignale,¹⁶ both for the homogeneous and the inhomogeneous case. The results of this calculation for $q/q_c = 2.02$ and $q/q_c = 2.71$ are plotted in Fig. 9, together with the experiment. When comparing Fig. 8 with Fig. 9, one sees clearly that taking into account lifetime effects is a step in the correct direction. The overall shape of the spectra has changed, so that the center of gravity of the calculated curves is shifted to smaller energy transfer ω . The steep rise of $\Gamma(p)$ at p_0 (see Sec. II) leads to the division of the spectra into two parts. If the momentum p of the final state [see Eq. (10)] is smaller than p_0 , and this applies to lower values of ω , damping is rather weak, so that the shape of the spectra are left nearly unchanged compared to RPA. If p is larger than p_0 , damping is large and the spectra become broadened for higher values of ω , which gives rise to the drastic change of their shape compared to RPA.

But in spite of the improved approach of the calculated curves to the experimental ones by including lifetime effects, an appreciable discrepancy is still left. This can be removed to a large extent by taking into account exchange and correlation via the static approximation $G(\mathbf{q})$ of the local-field factor $G(\mathbf{q}, \omega)$, as given in an analytic form by Ichimaru and Utsumi.³⁹ The local-field factor, used in our model calculation, is given in Fig. 10. It was shown

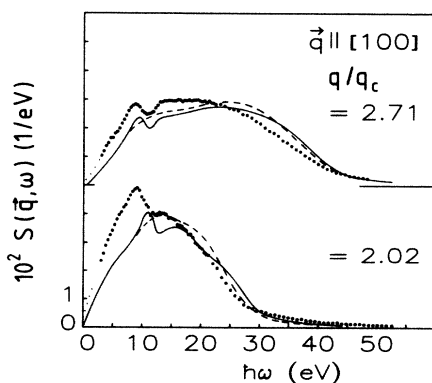


FIG. 9. Calculated $S(\mathbf{q}, \omega)$ including momentum-dependent lifetime for $\mathbf{q} \parallel [100]$; $q/q_c = 2.02$ and $q/q_c = 2.71$: dashed line, homogeneous electron liquid; solid line, pseudopotential band structure; and dots, experimental values.

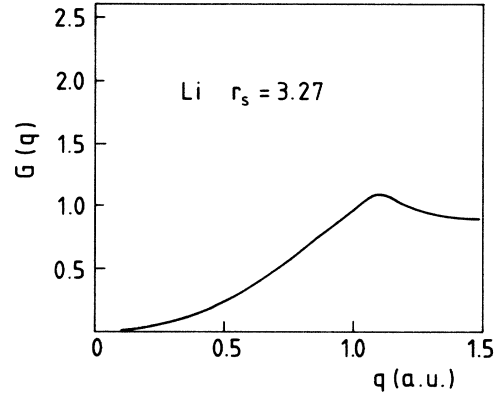


FIG. 10. Static local-field factor $G(q)$ according to Ref. 39 for the electron density of Li ($r_s = 3.27$).

that this rather simple way of introducing exchange and correlation conserves the f sum rule within the accuracy of our model calculations, 3%.

Finally, in addition, the ion-core polarizability was allowed for in an approximate manner by adding simply the electronic part of the free ion polarizability to ϵ_1 , which gives for Li a contribution of 0.017 (see Pirenne and Kartheuser⁵⁵). This procedure will change the first frequency moment of $S(\mathbf{q}, \omega)$ by a factor of $f(q)$ with respect to the pure valence electron value of $S(\mathbf{q}, \omega)$. By this factor $f(q)$ also the normalization of the experimental values has to be changed, as already indicated in Eq. (16). In all cases $f(q)$ deviated from unity by less than 2%.

The results of these calculations, which include lifetime and local-field corrections, again for $\mathbf{q} \parallel [100]$; $q/q_c = 2.02$ and $q/q_c = 2.71$, are given in Fig. 11. Compared with Fig. 9, the agreement between experiment and inhomogeneous model calculation is substantially improved.

In the Figs. 12–14, all experimental results for $q > q_c$ are confronted with their theoretical counterparts, which were calculated by taking into account pseudopotential

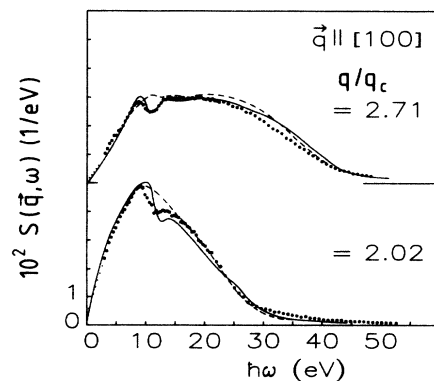


FIG. 11. Calculated $S(\mathbf{q}, \omega)$ including momentum-dependent lifetime, static local-field correction, and core polarizability for $\mathbf{q} \parallel [100]$; $q/q_c = 2.02$ and $q/q_c = 2.71$: dashed line, homogeneous electron liquid; solid line, pseudopotential band structure; and dots, experimental values.

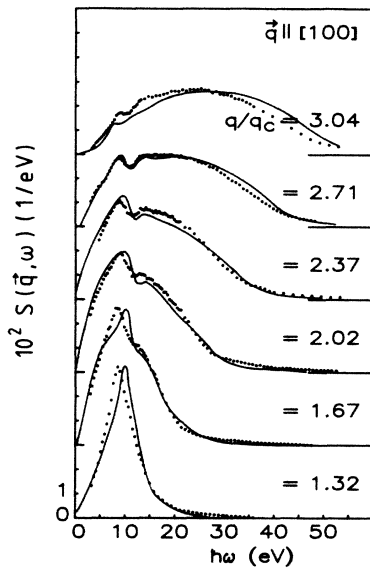


FIG. 12. Model calculated $S(\mathbf{q},\omega)$ including momentum-dependent lifetime, static local-field correction and core polarizability (solid line) together with experiments for $q > q_c$, $\mathbf{q}||[100]$ (dots).

band structure, momentum-dependent lifetime, exchange and correlation via the static local-field factor, and core polarizability.

Evaluating this confrontation of the experiment with calculations one can state the following:

(i) In spite of the fact that our model calculations are neither first principles nor self-consistent, the agreement between experiment and model with respect to the overall shape of the spectra is rather good. Therefore, the way we have introduced lifetime and local-field corrections seems to be correct, in principle, and reflects a proper understanding of the basic physical phenomena, even though the approximations used did not originate from a com-

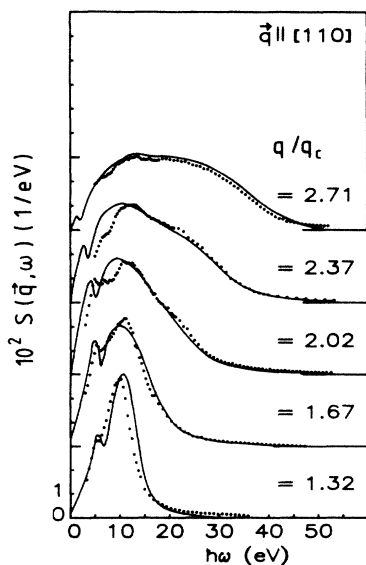


FIG. 13. Same as Fig. 12, but for $\mathbf{q}||[110]$.

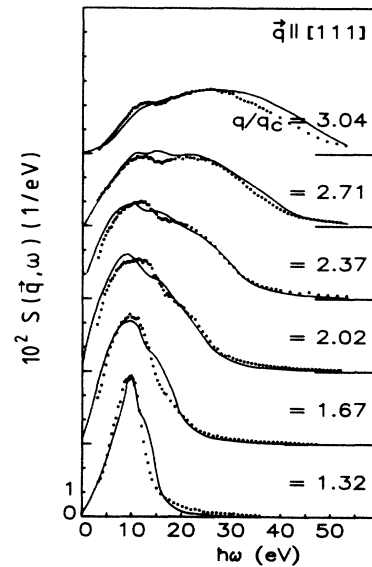


FIG. 14. Same as Fig. 12, but for $\mathbf{q}||[111]$.

mon first-principles base. But it should be stressed that our model calculations are free of adjustable parameters, which gives the agreement with experiment a certain quality.

(ii) This agreement is not only found for the overall shape but also for the most prominent orientation dependent special features, as the occurrence of the first ZBCS-related peaks and their adjacent dips in the [100] and the [110] spectrum, respectively.

(iii) The experimental position of the band-gap-connected peaks in the [100] spectra is not exactly reproduced by our model calculations. The same is true, but to a much less extent, with the band-gap-connected peaks in the [110] spectra. That is not surprising, since one cannot assume that a simple local pseudopotential calculation can yield exact values for the absolute energetic position of the bands, which are closely related to the way exchange and correlation are introduced into the band calculation. In order to demonstrate that a more sophisticated band calculation would give a much better agreement with experiment, the following estimation is presented.

The [100] ZBCS-like peak is attributed to a band gap across the (200) Bragg plane around the H point of the Brillouin zone. Moreover, it is well-known from our two-band calculations that a ZBCS at the top of its dispersion is always near the lower edge of the excitation gap (see Fig. 2). $E(H_{15})$ determines the lower edge of the excitation gap for transitions to the (200) Bragg plane. $E(H_{15})$ has a distance ΔE_1 of 9.6 eV from $E(\Gamma_1)$ in a first-principles band-structure calculation of Ref. 53, but a distance ΔE_2 of 11.1 eV in our pseudopotential approach. ΔE_2 is to ΔE_1 nearly as our model calculated to the experimental ZBCS peak position at $q/q_c = 2.02$, namely 10.0 eV:8.8 eV.

This, together with our model calculation, the result of which are presented in Figs. 12–14, gives us good confidence, that the first peak in both the [100] and the [110] spectra are due to corresponding gaps across the (200) and

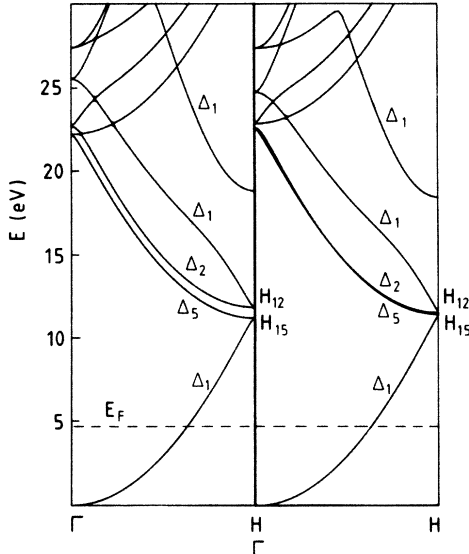


FIG. 15. Li band structure: left part, $V_{200}=0.055$ a.u., with splitting of the Δ_2 and Δ_5 band; and right part, $V_{200}=0.04$ a.u., with no splitting of Δ_2 and Δ_5 band.

the (110) Bragg plane, respectively. Additionally, the high sensitivity of the $S(\mathbf{q},\omega)$ spectra to details of the band structure can be demonstrated in the following way. If one reduces only the V_{200} pseudopotential coefficient in our model from 0.055 a.u. to 0.04 a.u., the energy split between the doubly degenerated Δ_5 band and the Δ_2 band goes to zero, as shown in Fig. 15. Coupled with this comparatively small variation in the band structure, there is a drastic change of the model $S(\mathbf{q},\omega)$ as shown in Fig. 16. The characteristic peak structure of the [100] spectra has disappeared due to closing the excitation gap, which arises for $\mathbf{q}||[100]$ as a consequence of the Δ_2 - Δ_5 splitting. This again is a strong indication that the fine structure of the [100] spectra is ZBCS-like.

(iv) Nevertheless it must be conceded that the discrepancy between the experiment and our calculation does not only refer to the absolute peak position in the [100] and [110] spectra but also to the peak dispersion. The experimental position of the corresponding first peak exhibits much less dispersion than the calculated one. To

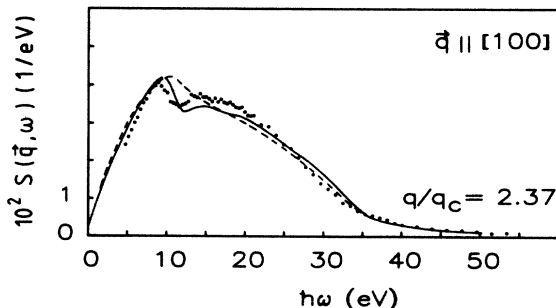


FIG. 16. Calculated $S(\mathbf{q},\omega)$ (lifetime, local-field correction, and pseudopotential band structure): solid line, $V_{200}=0.055$ a.u.; dashed line, $V_{200}=0.04$ a.u.; and dots, experimental values.

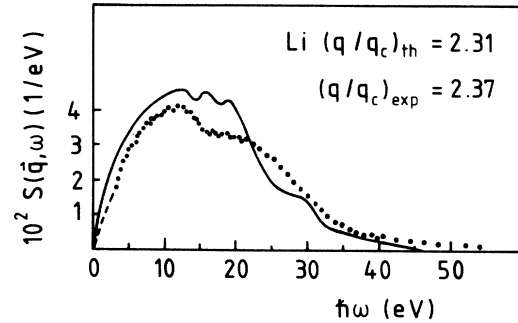


FIG. 17. Experiment $S(\mathbf{q},\omega)$ of Li for $q=2.37q_c$; $\mathbf{q}||[111]$ (dots). Calculated $S(\mathbf{q},\omega)$ of Ref. 24 for an homogeneous electron liquid of the density of Li for $q=2.31q_c$, normalized according to the f sum rule and convoluted with the experimental resolution.

some extent this may be due to the fact that our calculations do not take into account the real part of the momentum-dependent self-energy whereas its imaginary part is considered. Allowing for this real part by using its values for the homogeneous case as given by Lundquist⁴⁹ would counteract the discrepancy as far as peak dispersion is concerned, but without resulting in a full agreement.

(v) Although the experimental data have a statistical accuracy of nearly 1%, no indication of a fine structure of the order of 5% was found at positions, where it is predicted quite recently by Green, Neilson, and Szymanski²⁴ for $S(\mathbf{q},\omega)$ of a homogeneous electron liquid. This is demonstrated by means of Fig. 17, where our experimental $S(\mathbf{q},\omega)$ for $\mathbf{q}||[111]$ and $q=2.37q_c$ is confronted with the theoretical result of Ref. 24 which is for $q=2.31q_c$, somewhat less than the experimental momentum transfer but still within its error bar. The [111] direction has been chosen for comparison, since it is the directional profiles with the least indication of crystal-lattice effects. The theoretical curves have been normalized in the same way as our experimental ones according to the f sum rule [see Eq. (16)] and have been convoluted with the experimental resolution. But it is not only the absence of the theoretically predicted fine structure that leads to discrepancies between the experiment and the calculations of Ref. 24. Also the overall shape exhibits significant differences.

(vi) It must be conceded that the agreement between our calculations and the experiment is worse for $\mathbf{q}||[111]$, compared with the other \mathbf{q} directions. It is mainly an additional structure in the calculated spectra near 16 eV, which appears as a shoulder for small q and as an additional weak peak for larger q , and which makes the agreement worse. This structure cannot be found in the experiment. Since this structure exhibits only very weak dispersion it could be attributed to an incorrect calculation of the unoccupied states, as far as they contribute mainly to the [111] spectra. Thus the most prominent structure in the [111] spectra, the dip between 16 and 18 eV for $q/q_c > 2$, cannot be interpreted as due to band structure, and it remains possible that this dip is brought about by the steep rise of inverse lifetime at p_0 (see Fig. 1), as

predicted in Ref. 16, particularly because there is also a very weak indication of a dip in the [110] spectra nearly at the same position. On the other hand, the corresponding dip in the [100] spectra, which is at quite another position, appears to be a band-structure effect.

(vii) There is a distinct deviation of the calculated structure factors from the experimental ones at their high- ω side for $q/q_c > 2.4$. The deviation increases, if this part of the valence electron spectra approaches the onset of the core contribution at 55 eV. This discrepancy seems to be due to the contribution of the core electrons to ϵ_1 . This contribution increases with ω for an energy transfer that is smaller than the energetic onset position of the core-electron contribution to ϵ_2 . In terms of the Kramers-Kronig relation between ϵ_1 and ϵ_2 , this special ω dependence of the core contribution to ϵ_1 is a direct consequence of the edgelike structure of ϵ_2 at 55 eV and will diminish $S(\mathbf{q}, \omega)$ compared to our model calculation, which takes into account only an ω -independent contribution of the core to ϵ_1 .

VI. CONCLUSIONS

(i) Inelastic scattering of synchrotron x-ray radiation has proved to be a very valuable tool for investigating the dynamical structure of electrons in solids, especially for the range of larger momentum transfer.

(ii) In the case of Li metal, it seems to be well established that crystal-lattice effects produce a great deal of fine structure of the dynamical structure factor $S(\mathbf{q}, \omega)$ for $q > q_c$. Most of this fine structure can be attributed to gaps or deep valleys in the combined density of states for certain directions of momentum transfer \mathbf{q} as a consequence of energy gaps across Bragg planes perpendicular to \mathbf{q} .

(iii) The strong momentum dependence of the inverse quasiparticle lifetime of electrons with an edgelike in-

crease at a momentum, where decay of quasiparticles into a plasmon becomes possible, produces the characteristic overall shape of the spectra for $q > q_c$; that is, (a) the peak shift to smaller values of energy transfer ω compared with the position of the pure RPA peak, (b) the survival of crystal-lattice-induced fine structure only for the region of smaller energy transfer. Whether the two regions of very different lifetime of quasiparticle states are separated by a dip for larger q 's, as assumed in Ref. 16, was not finally decided by the experiment, because of strong overlap of this possible dip with lattice-induced structure for certain directions of \mathbf{q} .

(iv) Exchange and correlation corrections to the calculated $S(\mathbf{q}, \omega)$ spectra were needed, in order to bring them into final agreement with the experiment. This correction can be done by using the static approximation to the local-field factor.

(v) Remaining discrepancies between model calculated $S(\mathbf{q}, \omega)$ spectra and the experiment are mainly due both to a partly incorrect band structure, insofar as the exact energetic position of the bands is concerned, and to inadequate representation of the core polarization near the K edge. Possibly also the violation of particle number conservation in our handling of lifetime corrections can attribute to discrepancies.

ACKNOWLEDGMENTS

We thank U. Bonse, K. Fischer, S. Krasnicki, A. Millhouse, H. Schenk-Strauss, K. Hinz, Th. Risse, R. Nusshardt, U. Dretzler, and G. Ernst for valuable help with the measurements at DORIS/HASYLAB (Hamburger Synchrotronstrahlungslabor, Deutsches Elektronensynchrotron), K. Sturm for helpful discussions, and the Bundesminister für Forschung und Technologie (Bonn, Germany) for financial support.

¹P. Zacharias, *J. Phys. F* **5**, 645 (1975).

²P. E. Batson, C. H. Chen, and J. Silcox, *Phys. Rev. Lett.* **37**, 937 (1976).

³H. J. Höhberger, A. Otto, and E. Petri, *Solid State Commun.* **16**, 175 (1975).

⁴E. Petri and A. Otto, *Phys. Rev. Lett.* **34**, 1283 (1975).

⁵C. H. Chen and J. Silcox, *Phys. Rev. B* **16**, 4246 (1977).

⁶K. Sturm and L. E. Oliveira, *Phys. Rev. B* **30**, 4351 (1984).

⁷E.-Ni Foo and J. J. Hopfield, *Phys. Rev.* **173**, 635 (1968).

⁸P. M. Platzman and P. Eisenberger, *Phys. Rev. Lett.* **33**, 152 (1974).

⁹P. Eisenberger, P. M. Platzman, and P. Schmidt, *Phys. Rev. Lett.* **34**, 18 (1975).

¹⁰W. Schülke and W. Lautner, *Phys. Status Solidi B* **66**, 211 (1974).

¹¹G. D. Priftis, J. Boviatsis, and A. Vradis, *Phys. Lett.* **68A**, 482 (1978).

¹²W. Schülke, H. Nagasawa, and S. Mourikis, *Phys. Rev. Lett.* **52**, 2065 (1984).

¹³G. Mukhopadhyay, R. K. Kalia, and K. S. Singwi, *Phys. Rev. Lett.* **34**, 950 (1975).

¹⁴P. Vashishta and K. S. Singwi, *Phys. Rev. B* **6**, 875 (1972).

¹⁵B. K. Rao, S. S. Mandl, and D. N. Tripathy, *Phys. Lett.* **71A**, 447 (1979).

¹⁶S. Rahman and G. Vignale, *Phys. Rev. B* **30**, 6951 (1984).

¹⁷G. Niklasson, A. Sjölander, and F. Yoshida, *J. Phys. Soc. Jpn.* **52**, 2140 (1983).

¹⁸K. Awa, H. Yasuhara, and T. Asaki, *Solid State Commun.* **38**, 1285 (1981); *Phys. Rev. B* **25**, 3670 (1982).

¹⁹H. Mori, *Prog. Theor. Phys.* **33**, 423 (1965).

²⁰G. Mukhopadhyay and A. Sjölander, *Phys. Rev. B* **17**, 3589 (1978).

²¹H. De Raedt and B. De Raedt, *Phys. Rev. B* **18**, 2039 (1978).

²²E. Pajanne, *J. Phys. C* **15**, 5629 (1982).

²³F. Green, D. N. Lowy, and J. Szymanski, *Phys. Rev. Lett.* **48**, 638 (1982).

²⁴F. Green, D. Neilson, and J. Szymanski, *Phys. Rev.* **31**, 2779 (1985); **31**, 2796 (1985); **31**, 5837 (1985).

²⁵K. Utsumi and S. Ichimaru, *Phys. Rev. B* **23**, 3291 (1981).

²⁶K. C. Pandey, P. M. Platzman, and P. Eisenberger, *Phys. Rev. B* **9**, 5046 (1974).

²⁷S. P. Singhal, *Phys. Rev. B* **14**, 2352 (1976).

²⁸M. S. Haque and K. L. Kliewer, *Phys. Rev. B* **7**, 2416 (1973).

²⁹M. Taut and W. Hanke, *Phys. Status Solidi B* **77**, 543 (1976).

- ³⁰D. M. Miliotis, Phys. Rev. B **3**, 701 (1971).
³¹P. Nozières and D. Pines, Phys. Rev. **113**, 1254 (1959).
³²D. Pines and P. Nozières, *The Theory of Quantum Liquids* (Benjamin, New York, 1966), Vol. 1.
³³J. Lindhard, K. Dan. Vidensk. Selsk. Mat.-Fys. Medd. **28**, 8, 1 (1954).
³⁴K. S. Singwi, M. P. Tosi, R. H. Land, and A. Sjölander, Phys. Rev. **176**, 589 (1968).
³⁵K. S. Singwi, A. Sjölander, M. P. Tosi, and R. H. Land, Phys. Rev. B **1**, 1044 (1970).
³⁶J. J. Quinn, Phys. Rev. **126**, 1453 (1962).
³⁷N. D. Mermin, Phys. Rev. B **1**, 2362 (1970).
³⁸J. Hubbard, Proc. R. Soc. London, Ser. A **243**, 336 (1957).
³⁹S. Ichimaru and K. Utsumi, Phys. Rev. B **24**, 7385 (1981).
⁴⁰K. Utsumi and S. Ichimaru, Phys. Rev. B **22**, 1522 (1980); **22**, 5203 (1980); **24**, 3220 (1981).
⁴¹D. M. Ceperley and B. J. Alder, Phys. Rev. Lett. **45**, 566 (1980).
⁴²N. Wiser, Phys. Rev. **129**, 62 (1963).
⁴³W. M. Saslow and G. F. Reiter, Phys. Rev. B **7**, 2995 (1973).
⁴⁴P. M. Platzman and P. A. Wolff, *Waves and Interactions in Solid State Plasmas* (Academic, New York, 1973).
⁴⁵H. Ehrenreich and M. H. Cohen, Phys. Rev. **115**, 786 (1959).
⁴⁶W. Schülke and H. Nagasawa, Nucl. Instrum. Methods **222**, 203 (1984).
⁴⁷U. Bonse *et al.*, Acta Crystallogr. Sec. A (Suppl.) **40**, C-410 (1984).
⁴⁸W. Schülke, Nucl. Instrum. Methods (to be published).
⁴⁹B. I. Lundquist, Phys. Kondens. Mater. **7**, 117 (1968).
⁵⁰K. Sturm, Adv. Phys. **31**, 1 (1982).
⁵¹C. Kunz, Z. Phys. **196**, 311 (1966).
⁵²G. Paasch, Phys. Status Solidi **38**, K123 (1970).
⁵³H. Bross and G. Bohn, Z. Phys. B **20**, 261 (1975).
⁵⁴V. Heine and I. Abarenkov, Philos. Mag. **9**, 451 (1964).
⁵⁵J. Pirenne and E. Kartheuser, Physica **20**, 2005 (1964).